2

Morphology and substructure of martensite in steels

T. MAKI, Kyoto University, Japan

Abstract: Martensite in ferrous alloys exhibits various morphologies, chiefly lath, lenticular and thin plate, depending on chemical compositions and M_s temperature. This chapter reviews crystallographic features and substructures for each of these specific forms. Furthermore, the chapter discusses crystallographic features of packet and block in lath martensite, the origin of dislocation structure in lath and lenticular martensites, and the origin of the midrib in lenticular martensite.

Key words: morphology of ferrous martensite, lath martensite, lenticular martensite, thin plate martensite, substructure of ferrous martensite.

2.1 Morphology and crystallographic features of martensite in ferrous alloys

In ferrous alloys, an FCC austenite (γ) phase is transformed into three kinds of martensites with different crystal structures, depending on alloying elements and compositions, i.e., (1) $\gamma \rightarrow \alpha'$ (BCC or BCT) martensite, (2) $\gamma \rightarrow \varepsilon$ (HCP) martensite, and (3) $\gamma \rightarrow$ FCT martensite. The α' type martensite is the most common in ferrous martensites, and is formed, for example, in Fe-C and Fe-Ni alloys. The ε martensite is formed only in ferrous alloys with low-austenite stacking fault energy, such as Fe-Cr-Ni and Fe-high Mn alloys. Lastly, FCT martensite is very rare and has been found only in Fe-~30at%Pd and Fe-~25at%Pt alloys (Sohmura *et al.*, 1980; Oshima *et al.*, 1985).

The morphology of ε and FCT martensite is of a parallel-sided thin plate-type with planar interfaces. However, in the case of α' martensite, five different types of morphologies have been reported, i.e., lath, butterfly, $\{225\}_\gamma$-plate type, lenticular, and thin plate. Figure 2.1 (Maki, 1990) shows optical micrographs of α' martensite with different morphologies (a)–(e), and ε martensite (f). These five types of α' martensites have their own formation temperature. Figure 2.2 (Maki and Tamura, 1984) shows the formation range of various types of α' martensite as a function of martensite start temperature (M_s) and carbon content in Fe-Ni-C alloys. In the case of Fe-Ni-C alloys, four types of α' martensite are formed; only $\{225\}_\gamma$-plate type martensite is not found. Lath martensite forms at the highest temperatures, whilst thin plate martensite forms at the lowest temperatures. The transition temperature

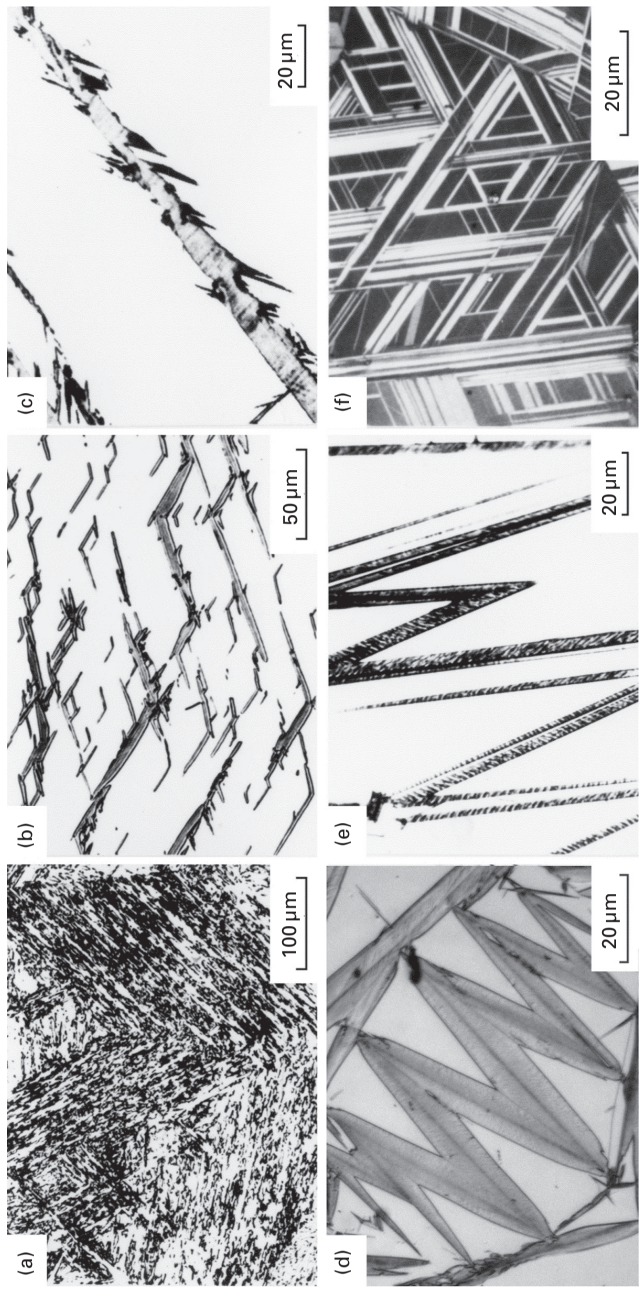

2.1 Optical micrographs of various types of martensites in ferrous alloys: (a) lath α' (Fe-7%Ni-0.22%C), (b) butterfly α' (Fe-20%Ni-0.73%C), (c) $(225)_\gamma$ plate type α'(Fe-8%Cr-0.9%C), (d) lenticular α' (Fe-29%Ni-0.26%C), (e) thin plate α' (Fe-31%Ni-0.23%C), (f) ε martensite (Fe-24%Mn) (Maki, 1990).

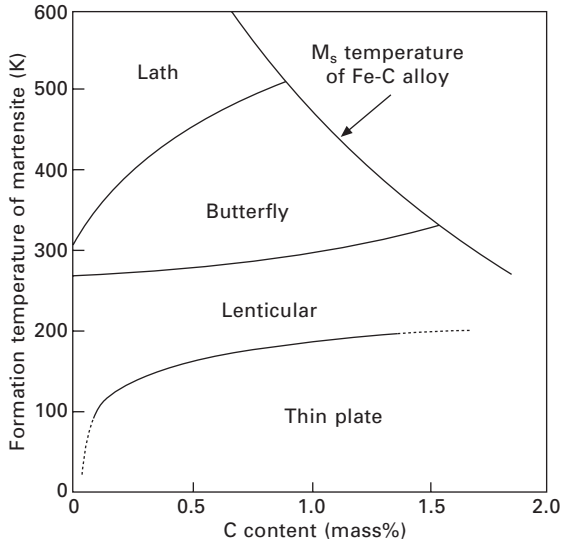

2.2 Formation range of various types of α' martensite (lath, butterfly, lenticular and thin plate) as a function of formation temperature (M_s) and carbon content in Fe-Ni-C alloys (Maki and Tamura, 1984).

of martensite morphology, from lenticular to thin plate, is increased with an increase in carbon content. For Fe-Ni binary alloys, the thin plate martensite does not form even at 77K. These α' martensites can be distinguished not only morphologically but also crystallographically. Thus, Table 2.1 (Maki, 1990) summarizes the substructures, habit planes (HP), and orientation relationships (OR) for the five types of α' martensite. With a decrease in M_s temperature, the substructure of α' martensite changes from dislocated (lath martensite) to twinned (thin plate martensite), and the habit plane changes from $\{111\}_\gamma$ to $\{225\}_\gamma$ and $\{3\ 15\ 10\}_\gamma$. Furthermore, the orientation relationship changes from K-S (Kurdjumov–Sachs) to N-W (Nishiyama–Wasserman) and G-T (Greninger–Troiano). Lath martensite nearly satisfies the K-S relationship with respect to austenite, and its habit plane is close to $\{111\}_\gamma$ or $\{557\}_\gamma$. Meanwhile, the habit plane of thin plate martensite is close to $\{3\ 15\ 10\}_\gamma$, and the orientation relationship approximates to the G-T relationship. These crystallographic features of thin plate martensites (Greninger and Troiano, 1949; Miyamoto *et al.*, 2009) are well explained by the phenomenological theory of martensite crystallography (Wechsler *et al.*, 1953; Bowles and Mackenzie, 1954) and are described in detail in Chapter 1 of this volume. The substructure and crystallography of lenticular martensite, which forms in the intermediate temperature range between lath and thin plate, is fairly complicated, compared with lath and thin plate martensite, as shown later.

The factors that determine the morphology and substructure of α' martensite

Table 2.1 Morphology, substructure, habit plane, and orientation relationship of five types of α′ martensites in ferrous alloys

	Morphology	Substructure	Habit plane	Orientation relationship	M_S	Alloy
1	Lath	Dislocations	$(111)_A$ or $(557)_A$	K–S	High	
2	Butterfly	Dislocations + Twins	$(225)_A$	K–S		Fe-Ni-(C) Fe-Ni-Cr-(C)
3	(225) type plate	Dislocations + Twins	$(225)_A$	K–S		Fe-7Cr-1C Fe-5Mn-1C Fe-3Mn-3Cr-1C
4	Lenticular	Dislocations + Twins (Mid-rib)	$(259)_A$ or $(3\ 10\ 15)_A$	N–W G–T		
5	Thin-plate	Twins	$(3\ 10\ 15)_A$	G–T	Low	Fe-high Ni-C Fe-7Al-2C Fe-25 at%Pt Fe-Ni-Co-Ti

Source: Maki (1990).
K–S OR $(111)_A//(011)_M$, $[\bar{1}01]_A//[\bar{1}\,\bar{1}1]_M$
N–W OR $(111)_A//(011)_M$, $[1\bar{1}0]_A//[100]_M$
G–T OR $(111)_A$ 1° from $(011)_M$, $[\bar{1}01]_A$ 2.5° from $[\bar{1}\,\bar{1}1]_M$

remain poorly defined. However, the M_s temperature, the strengths of parent austenite and product martensite, the critical resolved shear stress for slip and twinning in martensite, and the stacking fault energy of austenite are considered to be important factors (Davies and Magee, 1971; Krauss and Marder, 1971; Maki *et al.*, 1972; Carr *et al.*, 1978).

Lath and lenticular are the two major morphologies of α′ martensite (Reed, 1967; Marder and Krauss, 1967; Krauss and Marder, 1971). Lath martensite is formed in Fe-C (<0.6% C), Fe-Ni (<28% Ni), and Fe-Mn (<10% Mn) alloys, and most heat-treatable commercial steels, and has overwhelming industrial significance because it is a basic structure of high strength steels. Lenticular martensite appears in Fe-high C (0.8–1.8% C) and Fe-high Ni (29–33% Ni) alloys. The other three α′ martensites are not common in ferrous alloys. The butterfly martensite is formed in Fe-Ni, Fe-Ni-Cr alloys (Maki *et al.*, 1972; Umemoto *et al.*, 1984). The $\{225\}_\gamma$-plate type martensite is formed in Fe-Cr-C alloys with a low-stacking fault energy of the parent austenite (Shimizu *et al.*, 1970).

The ε martensite is formed in Fe-Mn (15–27% Mn) (Schumann, 1967) and austenitic stainless steels, such as Fe-18%Cr-8%Ni alloy. This martensite contains a high density of stacking faults. Amongst the various martensites in ferrous alloys, thin plate α′ martensite and ε martensite have the possibility to exhibit a shape memory effect which is discussed in Chapter 4 of this volume.

2.2 Morphology and substructure of lath martensite

2.2.1 Crystallographic features of lath martensite

The size of martensite laths is very small, e.g., the lath width is usually of the order of 0.2–0.5 μm and, thus, individual laths are not clearly observed in optical micrographs. However, since lath martensites have a tendency to become aligned parallel to one another in a large region of the austenite grain (Fig. 2.3(a)), lath martensite exhibits a characteristic microstructure at the optical microscopic scale (Fig. 2.3(b)). Thus, the current view held is that the austenite grain is divided into packets (a group of parallel laths with the same habit plane) and that each packet is further subdivided into blocks (a group of laths of the same orientation, i.e., the same variant of the K-S orientation relationship), as is shown in Fig. 2.3(c) (Marder and Marder, 1969; Inoue *et al.*, 1970; Matsuda *et al.*, 1972). These packet and block

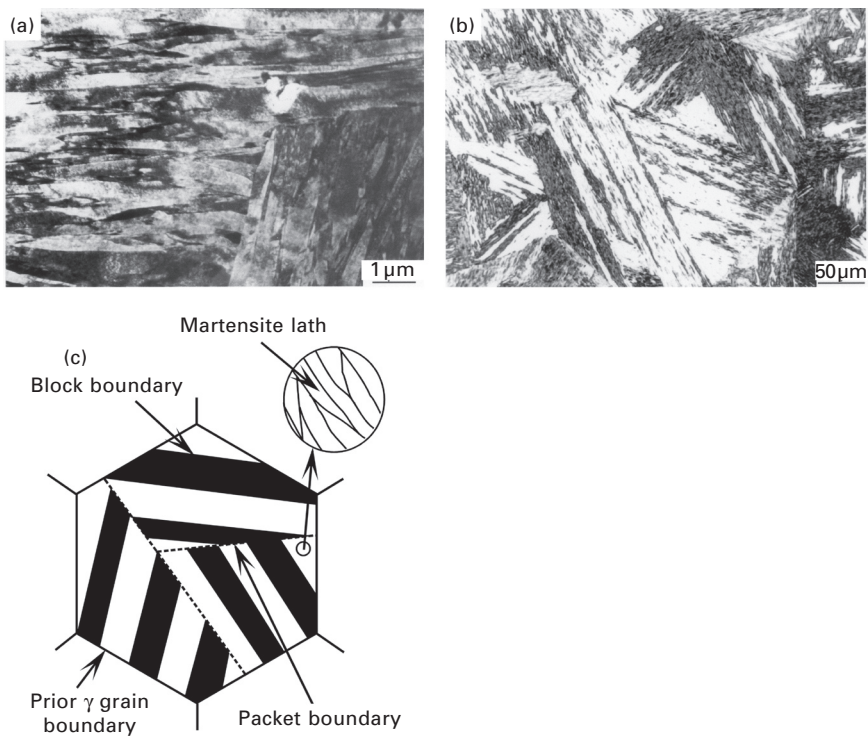

2.3 Transmission electron micrograph (a) and optical micrograph (b) of lath martensite in Fe-0.2%C alloy, and (c) schematic diagram showing characteristic morphology of lath martensite in an austenite grain (Marder and Marder, 1969; Inoue *et al.*, 1970; Matsuda *et al.*, 1972).

morphologies gradually change with carbon content, as shown schematically in Fig. 2.4 (Maki *et al.*, 1980). With an increase in carbon content of up to about 0.8%, the packet and blocks become finer, and are consequently more difficult to define in optical micrographs of high-carbon alloys. In the case of 0.8% C alloy, small amounts of lenticular martensite also form in addition to lath martensite.

Since the strength and toughness of martensitic steels are strongly related to packet and block sizes (the 'effective' grain size in a lath martensitic structure) (Inoue *et al.*, 1970; Matsuda *et al.*, 1972), the characteristics of the morphology and crystallography of lath martensite are of great importance and were studied extensively in the 1960s and 1970s. Recently, new and more accurate techniques for orientation measurement, with a margin of error less than 1°, such as Kikuchi diffraction patterns taken from a local area using the transmission electron microscope (TEM), and the electron back-scattered diffraction (EBSD) pattern from scanning electron microscopy (SEM), have been developed (Gourgues *et al.*, 2000; Zaefferer, 2003). Therefore, the crystallography of lath martensite in Fe-C alloys with different carbon contents has been re-examined using Kikuchi diffraction patterns and EBSD analysis (Morito *et al.*, 2003a, 2006).

As mentioned above, lath martensite has the K-S orientation relationship with respect to the austenite matrix. In the case of the K-S relationship, there are 24 variants as shown in Table 2.2. Laths with the same plane parallel relationship, e.g., V1–V6, have the same habit plane, e.g., $(111)_\gamma$ for V1–V6. As shown in Fig. 2.3(c), the packet consists of parallel laths with the same habit plane, and thus the same plane parallel relationship. Since there are four equivalent {111} austenite planes (i.e., (111), $(1\bar{1}1)$, $(\bar{1}11)$ and $(11\bar{1})$), there are four crystallographically different packets in any given austenite grain. In a packet, there are six variants (e.g., V1–V6) with different direction parallel relationships on the same conjugate parallel close-packed plane (e.g., $(111)_\gamma$ // $(011)_{\alpha'}$). Figure 2.5 shows the orientation relationship between austenite and the six K-S variants (V1–V6) within a packet. When V1 is taken as a reference, the orientation relationship between V1 and V2 is a twin relationship. Furthermore, variants 3, 5 or 6 are about 10–20° apart

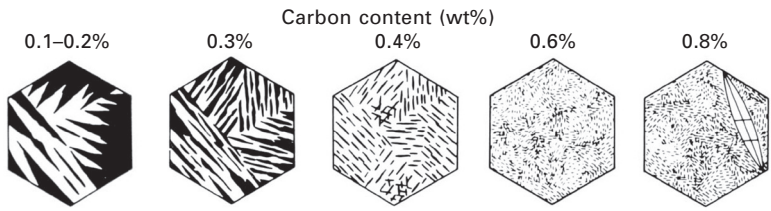

2.4 Schematic diagram showing a change in microstructure at the scale of the optical microscope of lath martensite with carbon content in Fe-C alloys (Maki *et al.,* 1980).

Table 2.2 Twenty-four variants in the K–S relationship

Variant no.	Plane parallel (Austenite)//(Martensite)	Direction parallel (Austenite)//(Martensite)
V1	$(111)_\gamma//(011)\alpha'$	$[\bar{1}01]_\gamma//[\bar{1}\,\bar{1}\,1]\alpha'$
V2	$(111)_\gamma//(011)\alpha'$	$[\bar{1}01]_\gamma//[\bar{1}1\bar{1}]\alpha'$
V3	$(111)_\gamma//(011)\alpha'$	$[01\bar{1}]_\gamma//[\bar{1}\,\bar{1}\,1]\alpha'$
V4	$(111)_\gamma//(011)\alpha'$	$[01\bar{1}]_\gamma//[\bar{1}1\bar{1}]\alpha'$
V5	$(111)_\gamma//(011)\alpha'$	$[1\bar{1}0]_\gamma//[\bar{1}\,\bar{1}\,1]\alpha'$
V6	$(111)_\gamma//(011)\alpha'$	$[1\bar{1}0]_\gamma//[\bar{1}1\bar{1}]\alpha'$
V7	$(1\bar{1}1)_\gamma//(011)\alpha'$	$[10\bar{1}]_\gamma//[\bar{1}\,\bar{1}\,1]\alpha'$
V8	$(1\bar{1}1)_\gamma//(011)\alpha'$	$[10\bar{1}]_\gamma//[\bar{1}1\bar{1}]\alpha'$
V9	$(1\bar{1}1)_\gamma//(011)\alpha'$	$[\bar{1}\,\bar{1}0]_\gamma//[\bar{1}\,\bar{1}\,1]\alpha'$
V10	$(1\bar{1}1)_\gamma//(011)\alpha'$	$[\bar{1}\,\bar{1}0]_\gamma//[\bar{1}1\bar{1}]\alpha'$
V11	$(1\bar{1}1)_\gamma//(011)\alpha'$	$[011]_\gamma//[\bar{1}\,\bar{1}\,1]\alpha'$
V12	$(1\bar{1}1)_\gamma//(011)\alpha'$	$[011]_\gamma//[\bar{1}1\bar{1}]\alpha'$
V13	$(\bar{1}11)_\gamma//(011)\alpha'$	$[0\bar{1}1]_\gamma//[\bar{1}\,\bar{1}\,1]\alpha'$
V14	$(\bar{1}11)_\gamma//(011)\alpha'$	$[0\bar{1}1]_\gamma//[\bar{1}1\bar{1}]\alpha'$
V15	$(\bar{1}11)_\gamma//(011)\alpha'$	$[\bar{1}0\bar{1}]_\gamma//[\bar{1}\,\bar{1}\,1]\alpha'$
V16	$(\bar{1}11)_\gamma//(011)\alpha'$	$[\bar{1}0\bar{1}]_\gamma//[\bar{1}1\bar{1}]\alpha'$
V17	$(\bar{1}11)_\gamma//(011)\alpha'$	$[110]_\gamma//[\bar{1}\,\bar{1}\,1]\alpha'$
V18	$(\bar{1}11)_\gamma//(011)\alpha'$	$[110]_\gamma//[\bar{1}1\bar{1}]\alpha'$
V19	$(11\bar{1})_\gamma//(011)\alpha'$	$[\bar{1}10]_\gamma//[\bar{1}\,\bar{1}\,1]\alpha'$
V20	$(11\bar{1})_\gamma//(011)\alpha'$	$[\bar{1}10]_\gamma//[\bar{1}1\bar{1}]\alpha'$
V21	$(11\bar{1})_\gamma//(011)\alpha'$	$[0\bar{1}\,\bar{1}]_\gamma//[\bar{1}\,\bar{1}\,1]\alpha'$
V22	$(11\bar{1})_\gamma//(011)\alpha'$	$[0\bar{1}\,\bar{1}]_\gamma//[\bar{1}1\bar{1}]\alpha'$
V23	$(11\bar{1})_\gamma//(011)\alpha'$	$[101]_\gamma//[\bar{1}\,\bar{1}\,1]\alpha'$
V24	$(11\bar{1})_\gamma//(011)\alpha'$	$[101]_\gamma//[\bar{1}1\bar{1}]\alpha'$

from a twin relation. These variants are high-angle with respect to V1. On the other hand, the misorientation between V1 and V4 is a low angle of about 10°. The V2/V5 and V3/V6 pairs are also combinations of low-angle misorientation.

Figures 2.6(a) and (b) (Morito *et al.*, 2003a) show a SEM image of a block structure within a packet of lath martensite in an ultra-low-carbon alloy, and the corresponding orientation image map obtained through EBSD analysis. Each block, with a little different contrast in SEM (Fig. 2.6(a)), corresponds to substantially different contrasts in the orientation image map (Fig. 2.6(b)). Blocks of B1, B2, and B3 with three different contrasts are formed repeatedly. It has been thought that the block consists of laths with a single variant, as shown in Fig. 2.3(c). However, Fig. 2.6(b) clearly shows that there are small regions showing slightly different contrasts, even in a given block, indicating that each block actually consists of two variants (termed sub-blocks), such as the combination of V1/V4, V3/V6 and V2/V5 with a small misorientation of about 10°. Figure 2.6(c) (Morito *et al.*, 2006) is an example of a TEM image showing that a block consists of two sets

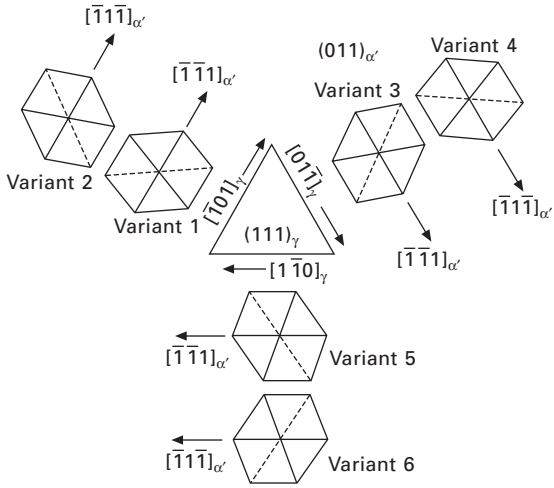

Variant no.	Misorientation from Variant 1 (V1)
V2	twin relation (∑3)
V3	10.53° from twin relation
V4	10.53°
V5	10.53° from twin relation
V6	21.06° from twin relation (∑11)

2.5 Orientation relationship between K-S variants (V1–V6) in a packet of lath martensite.

of sub-blocks. Two sets of parallel laths with V1 and V4 in a given block were observed. These variants are separated by a small misorientation of about 10°, and both variants can be distinguished by a slight difference in the habit plane, i.e., one is $(575)_\gamma$ and the other is $(755)_\gamma$, and both are close to the (111) austenite plane.

Figure 2.7 (Morito *et al.*, 2003a) shows a summary of the observations of a lath martensite structure in various Fe-C alloys. As carbon content increases, block and packet sizes decrease, as shown in Fig. 2.4. In low-carbon alloys (0–0.4% C, Fig. 2.7(a)), each packet consists of parallel blocks, and there are three blocks with different orientations in each packet. Furthermore, each block consists of laths of two specific variant groups (sub-blocks), which are misoriented by a small angle of about 10°. In high-carbon alloys (>0.6% C, Fig. 2.7(b)), packets consist of fine blocks in which the width is a few μm. The block consists of laths with a single variant, and six blocks with different orientations exist in a packet.

As shown above, blocks and packets are mostly surrounded by high-angle boundaries whereas lath boundaries in a block are of a low-angle type. Packets and blocks are important factors for both strengthening and toughening martensitic steels, as implied already. It is thus important that the size of the packets and blocks is shown to decrease as austenite grain

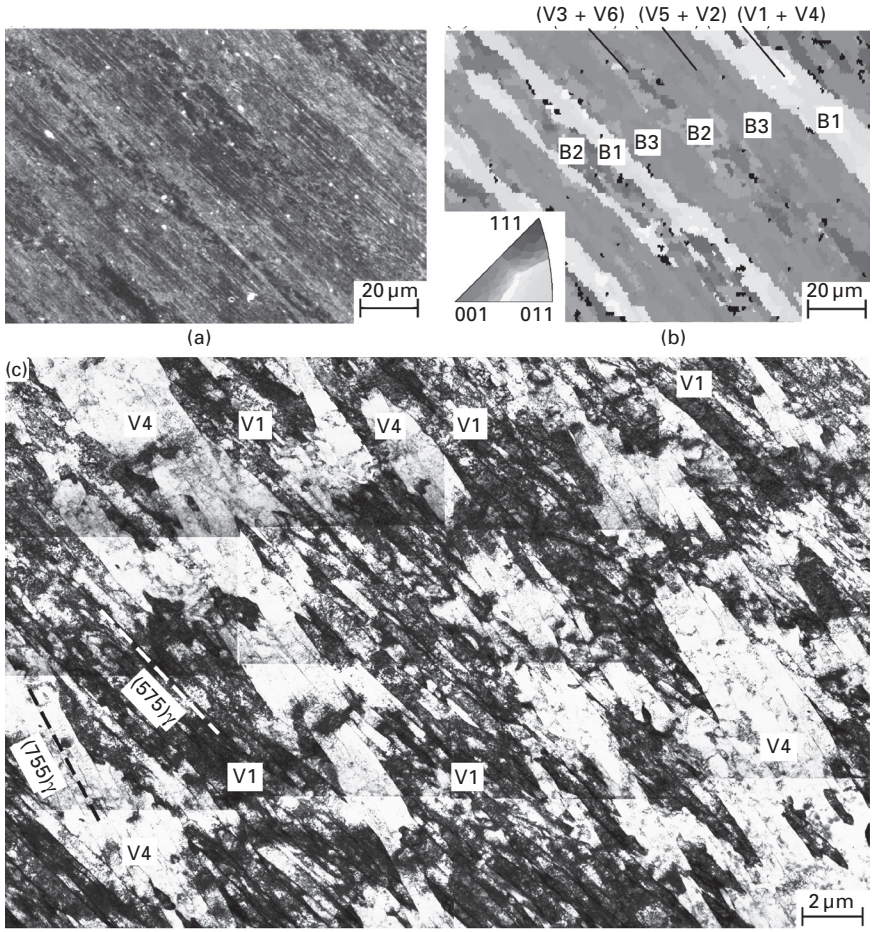

2.6 (a) Scanning electron micrograph of block structure within a packet of lath martensite in Fe-0.14%Mn-0.0026%C alloy, (b) corresponding crystal-orientation map measured by EBSD analysis, (c) transformation electron micrograph showing the block structure of lath martensite in Fe-3.1%Mn-0.004%C alloy. The block consists of two specific K-S variants (Morito *et al.*, 2003a).

size is refined, although the lath size is almost insensitive to changes in prior austenite grain size (Swarr and Krauss, 1976; Maki *et al.*, 1980; Morito *et al.*, 2005). Figure 2.8 (Furuhara *et al.*, 2008) is an example showing the relationship between prior austenite grain size and packet or block size in Fe-0.2%C alloys. Another way to decrease the packet and block sizes would be to increase the cooling rate (Tsuzaki and Maki, 1981), along with the partial formation of bainite before martensite transformation (Ohmori *et al.*, 1974). The bainite transformation effectively partitions the prior austenite

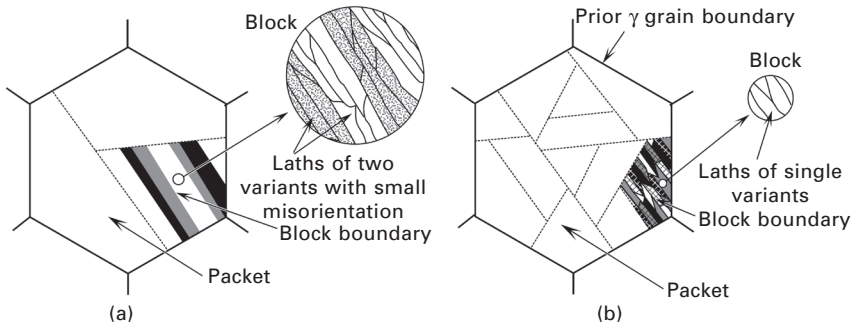

2.7 Schematic diagram showing lath martensite structure in (a) low-carbon (0–0.4% C) and (b) high-carbon (0.6% C) alloys (Morito *et al.*, 2003a).

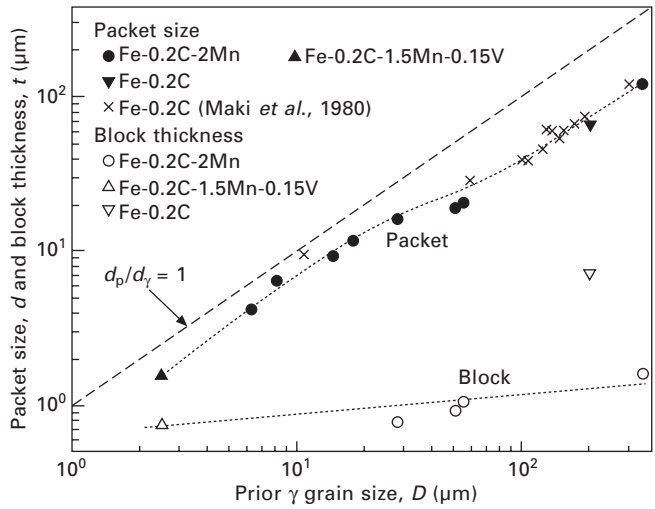

2.8 Variation of packet size and block width of lath martensite with austenite grain size in various low-carbon (0.2% C) alloys (Furuhara *et al.*, 2008).

grain before martensite forms, resulting in refinement of the packets of lath martensites.

2.2.2 Dislocation density of lath martensite

It is known that lath martensite shows very high dislocation densities in the order of 10^{14} or 10^{15} m^{-2}, which is similar to those of very heavily cold-worked alloys. However, quantitative studies on dislocation density in martensite are very few. One of the difficulties in the measurement of dislocation density

by TEM observation is the determination of thin foil thickness. Kehoe and Kelly (1970) determined foil thickness from extinction thickness fringes in an inclined boundary and measured the dislocation density in lath martensite of Fe-C alloys with carbon content from 0.01 to 0.1%. Thus it was shown that the dislocation density increases with carbon content. However, the effect of carbon content greater than 0.1% has not yet been made clear. Consequently, more recent measurements of dislocation density within lath martensite in Fe-C alloys (0–0.8% C) and Fe-Ni (0–23% Ni) alloys have been made by TEM, with precise determination of foil thickness using the convergent-beam electron diffraction (CBED) method (Morito *et al.*, 2003b).

Figure 2.9(a) (Morito *et al.*, 2003b) shows the change in dislocation density with carbon content in Fe-C alloys. As carbon content increases, the dislocation density increases. This tendency is similar to the results obtained by Kehoe and Kelly (1970) and subsequently also by Norström (1976) in low-carbon (0.01–0.1% C) martensites. It was also noted that the number of dislocations decreases slightly when carbon content increases from 0.6 to 0.8%. TEM observation revealed that laths in Fe-0.8%C alloys contained a higher fraction of fine transformation twins, whilst laths in Fe-0.6%C alloys also contained twins, but to a lesser extent. Therefore, it can be considered that the decrease in dislocation density is likely to be associated with this twinning, which occurs partly as a lattice invariant shear in the martensite transformation.

Figure 2.9(b) (Morito *et al.*, 2003b) shows the effect of Ni content on the dislocation density in Fe-Ni martensite. In this experiment, lath martensite is formed in the alloys with Ni contents of 0%, 11%, 15% and 23%, and lenticular martensite is formed in the Fe-31%Ni alloy. As the Ni content increases, the dislocation density in lath martensite increases slightly. However, this composition dependence in Fe-Ni alloys is very small, compared with Fe-C alloys. On the other hand, dislocation density in lenticular martensite in Fe-31%Ni alloys is lower than that of lath martensite in Fe-23%Ni alloy in the same way as for 0.8% C alloy in Fe-C alloys. This suggests that the occurrence of partial twinning results in the decrease of dislocation density in martensite. The composition dependence from 0 to 23% Ni on the dislocation density is similar to previous studies by Chaudhuri *et al.* (1972). However, they showed that dislocation density measured using X-ray diffraction increases sharply in the range of Ni content over 30%, which exhibits lenticular martensite, although the dislocation density measured using TEM is not so high. They concluded that this difference is caused by the loss of dislocations on thinning foils for TEM observation. If the effect of thin foil preparation exists, the dislocation density measured by TEM should always be lower than that measured using X-ray analysis. However, as shown in Fig. 2.9(b), their results regarding dislocation densities for lower Ni contents are nearly the same between X-ray and TEM measurements. Thus, it can be

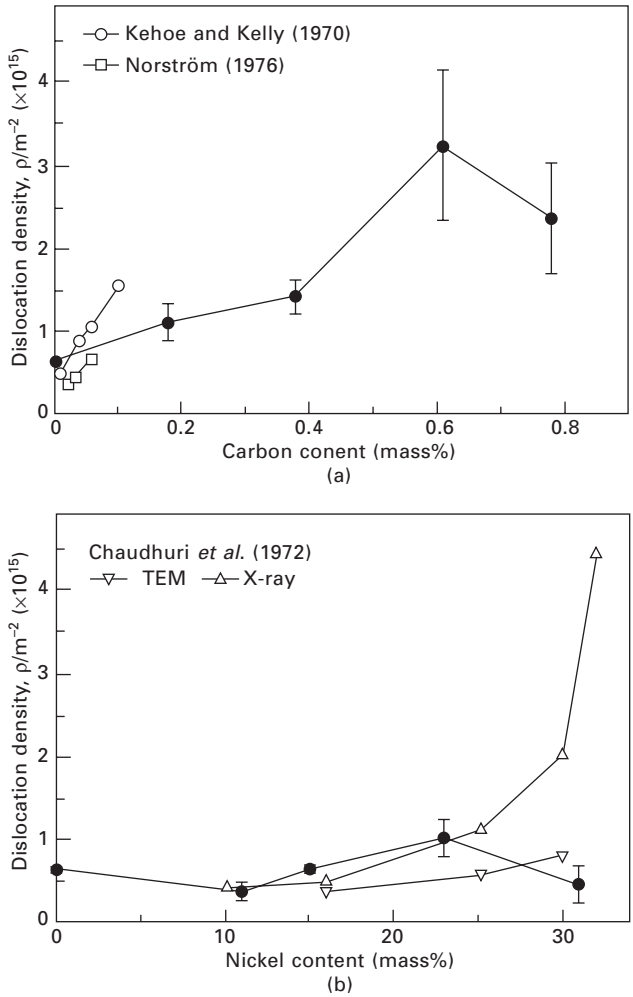

2.9 Change in dislocation density (a) in lath martensite with carbon content in Fe-C alloys, and (b) in lath martensite (Fe-0–23%Ni) and lenticular martensite (Fe-31%Ni) with Ni content in Fe-Ni alloys (Morito *et al.*, 2003b).

considered that the thin foil effect on dislocation density could be minimal. One of the possible reasons for this is the decrease in the mosaic particle size, due to the presence of fine transformation twins in lenticular martensite. This might result in the increase in the apparent dislocation density through the analysis of X-ray line-broadening.

2.3 Morphology and substructure of lenticular martensite

One of the features of lenticular martensite is the so-called 'burst' phenomenon, in which one martensite plate nucleates a sequence of plates, presumably as a result of stress concentrations set up when the first plate reaches an obstruction, such as a grain boundary or another martensite plate. As a result of burst transformation, lenticular martensite is formed as a zigzag array of plates, as shown in Fig. 2.1(d).

The shape of lenticular martensite varies with formation temperature, i.e., M_s temperature, as shown in Fig. 2.10(a) and (b) (Shibata *et al.*, 2009). The martensite (M)-austenite (A) interface in the Fe-32.9%Ni alloy (M_s = 171 K) is smooth. On the other hand, the M/A interface in the Fe-30.8%Ni alloy (M_s = 223 K) is quite irregular. Irrespective of boundary morphology, both martensites contain a straight line at the centre of the plate. This straight line (in reality, a plane) is called the 'midrib', and is considered to be the first part of a plate to form (Neuhauser and Pitsch, 1971; Kakeshita *et al.*, 1980). Since the M/A interface is not planar and does not have a definite habit plane, the midrib plane is usually taken as the habit plane of lenticular martensite, which is close to $\{2\ 5\ 9\}_\gamma$ or $\{3\ 10\ 15\}_\gamma$ (Reed, 1967; Krauss and Pitsch, 1965).

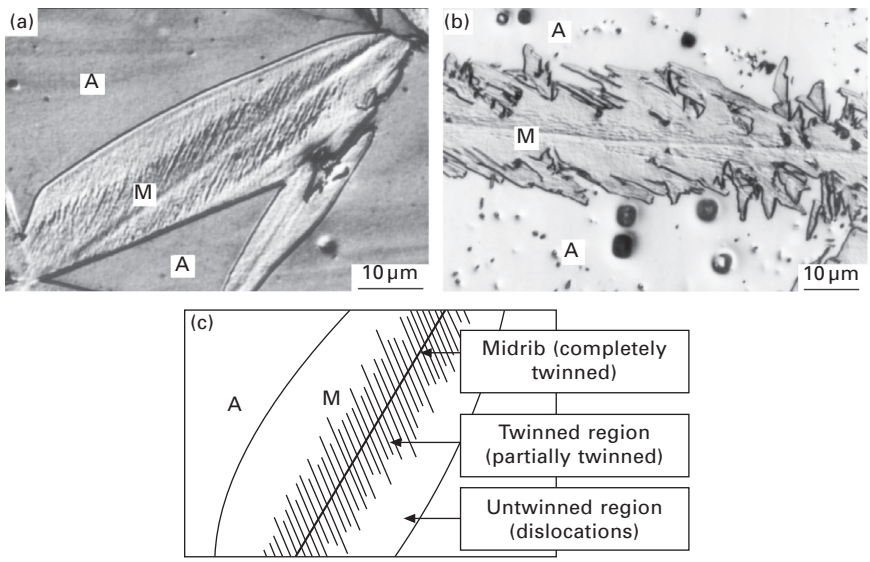

2.10 Optical micrographs of lenticular martensite in (a) Fe-32.9%Ni (M_s = 171 K), and (b) Fe-30.8%Ni (M_s = 223 K), and (c) schematic diagram of internal structure in lenticular martensite (Shibata *et al.*, 2009).

The substructure of lenticular martensite is more complicated compared with lath and thin plate martensite. As is shown schematically in Fig. 2.10(c), the lenticular martensite plate consists of three regions: (1) the 'midrib', which is completely twinned as thin plate martensite, (2) the 'twinned region', which partly consists of twins extending from the midrib, and (3) the 'untwinned (dislocated) region', which consists of a high density of dislocations. Even in an optical micrograph, the twinned regions can be recognized as a darkened area, as in Fig. 2.10(a), through suitable etching. It appears that the twinned region of lenticular martensite becomes thinner and the M/A interface more irregular when the M_s temperature increases.

Figure 2.11 (Shibata *et al.*, 2009) highlights TEM images showing the change in substructure from the midrib to the M/A interface in the

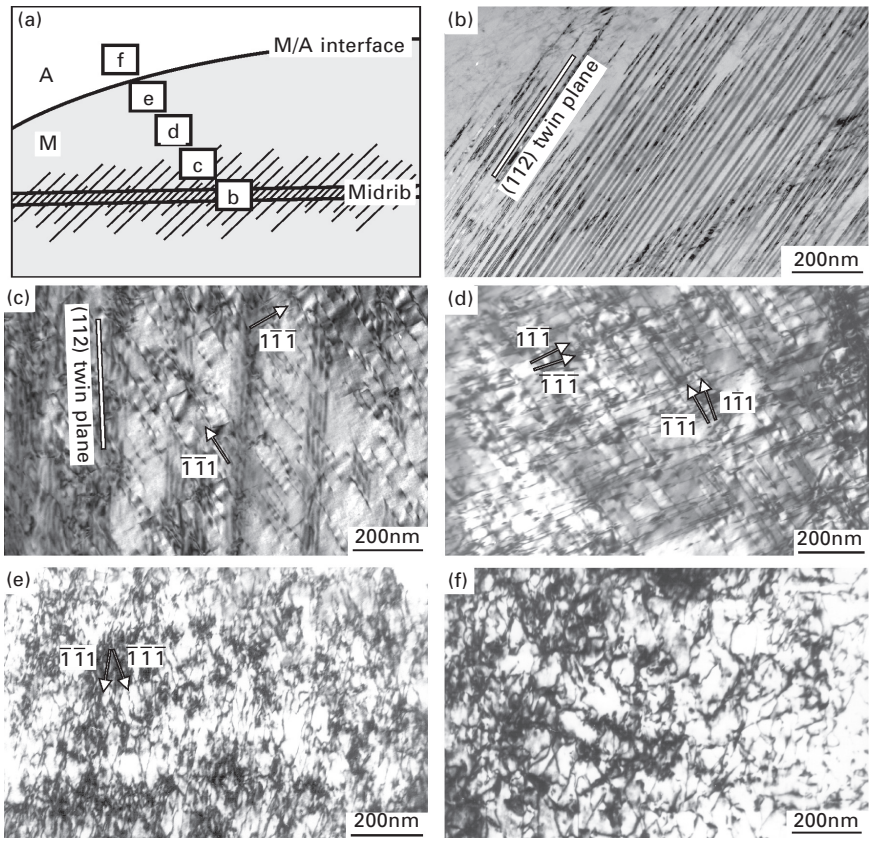

2.11 Transmission electron micrographs showing the substructure of lenticular martensite in Fe-32.9%Ni alloy: (a) schematic diagram describing the areas of observation, (b) midrib region, (c) twinned region, (d) untwinned region near the twinned region, (e) untwinned region near the M (martensite)/A (austenite) interface, and (f) surrounding austenite near the M/A interface (Shibata *et al.*, 2009).

lenticular martensite plate of an Fe-33%Ni alloy. The midrib region in Fig. 2.11(b), corresponding to 'b' in the schematic illustration in Fig. 2.11(a), is completely twinned. The twinning system is $(112)[\bar{1}\,\bar{1}1]_M$. In the twinned region corresponding to 'c' in Fig. 2.11(a), both fine twins and one set of screw dislocations, Burgers vector of which is parallel to the twinning shear direction, are observed as shown in Fig. 2.11(c). The structure in the untwinned region can be divided into two types, as shown in Figs 2.11(d) and 2.11(e). The area near the twinned region corresponding to 'd' in Fig. 2.11(a) contains several sets of screw dislocations (Fig. 2.11(d)). In contrast, the area near the M/A interface, corresponding to 'e' in Fig. 2.11(a), contains many tangled dislocations, in addition to straight dislocations (Fig. 2.11(e)). Figure 2.11(f) shows the dislocation structure in the surrounding austenite ('f' in Fig. 2.11(a)). The austenite contains a high density of tangled dislocations. These austenite dislocations might be introduced by the slip deformation for the accommodation of transformation strain. Because of the similarity of Figs 2.11(e) and (f), it can be considered that these austenite dislocations are inherited by the lenticular martensite during its growth.

The changes in the substructure of lenticular martensite in Fe-Ni alloys are shown by stages in Fig. 2.12 (1)→(2)→(3-1)→(3-2) (Shibata *et al.*, 2009). A midrib with a high density of $(112)[\bar{1}\,\bar{1}1]_M$ transformation twins is formed at the earliest stage of transformation (Fig. 2.12(1)). This is thin plate martensite itself, as is described later. In Fig. 2.12(2), the partial growth of twins in the midrib and the introduction of a set of screw dislocations with a Burgers vector of $a/2[\bar{1}\,\bar{1}1]_M$ accompanies the formation of the twinned region. These screw dislocations can be considered emissary dislocations decomposed from the transformation twins. The complete transition of lattice-invariant deformation, from twinning to slip during plate growth, results in the formation of an untwinned region (Fig. 2.12(3)). This untwinned region

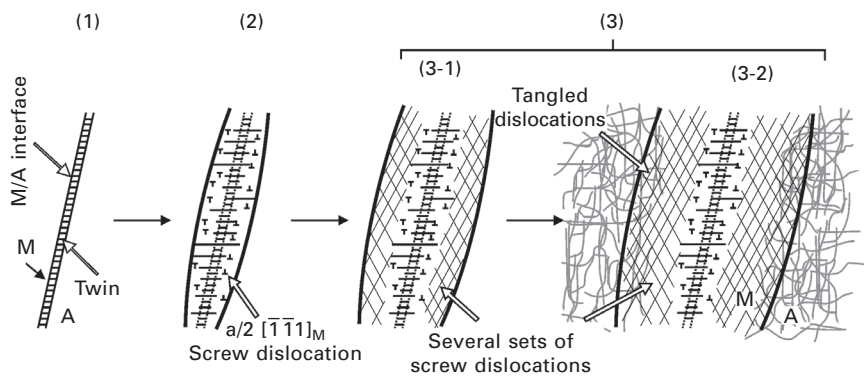

2.12 Schematic diagram showing the development of substructure during growth of lenticular martensite (Shibata *et al.*, 2009).

consists of two distinct regions with different substructures. At the growth stage ((3)-1), several sets of screw dislocations are observed that may result from lattice-invariant deformation. With further growth, plastic deformation also occurs in the surrounding austenite to accommodate the transformation strain. Because martensite inherits these accommodation dislocations in the parent austenite during growth, non-linear and tangled dislocations can be observed in the untwinned region near the M/A interface ((3)-2). The change in the lattice-invariant deformation mode from twinning to slip is likely to be caused by an increase in the local temperature produced by latent heat during martensite transformation, as proposed by Patterson and Wayman (1966).

It is common knowledge that the dislocation structure in an untwinned region of lenticular martensite consists of an array of uniformly distributed straight screw dislocations, as shown in Fig. 2.11(d). On the other hand, the dislocations in lath martensite are tangled and arranged in incipient dislocation cells as shown in Fig. 2.13(a). It has been considered that the dislocation tangles are a result of a plastic deformation mode consistent with the high M_s (a high-temperature range of formation) of low-carbon lath martensite. However, it should be emphasized that, even in lenticular martensite, the dislocation structure in an untwinned region close to the M/A interface is very similar to that of lath martensite. By careful observation, it has been confirmed that lath martensite definitely contains a set of straight screw dislocations, as shown in Fig. 2.13(b). Therefore, it can be considered that the dislocation structure in lath martensite consists of a set of screw dislocations, which are formed by the lattice invariant shear during transformation, along with tangled dislocations, which are inherited by martensite from the austenite matrix (Shibata *et al.*, 2009).

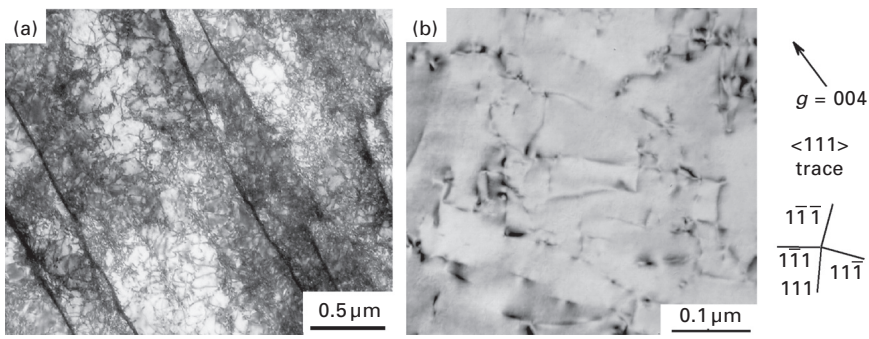

2.13 Transmission electron micrographs showing two types of dislocation structures in lath martensites (Fe-1.5%Mn-0.0026%C): (a) tangled dislocations, (dislocation cells) and (b) uniformly distributed straight dislocations.

2.4 Morphology and substructure of thin plate martensite

Figure 2.14 (Maki and Tamura, 1986) is a TEM image of thin plate martensite in Fe-Ni-C alloy. This martensite is characterized by a highly smooth and planar interface and the absence of a midrib, and (112) transformation twins in martensite extend completely from one interface to the other. In the case of α′ martensite with other types of morphologies, an A/M interface is not generally planar and no transformation twins exist in the martensite near an interface. Furthermore, it is characteristic that the parent austenite in the vicinity of thin plate martensite rarely contains dislocations. This indicates that no accommodation slip occurs there during martensitic transformation and that, therefore, the transformation strain is elastically accommodated by the austenite. This is in contrast to observations made regarding other types of α′ martensite (Miyamoto *et al*., 2009).

Each transformation twin in thin plate martensite extends completely, with uniform width, across the entire plate. On the other hand, the transformation twins in lenticular martensite are tapered, and thus the width of each twin decreases from the midrib as the M/A interface is approached (Maki and Wayman, 1976). Figure 2.15 (Maki and Wayman, 1976) shows the change in transformation twin width with carbon content in the thin plate martensite of Fe-Ni-C alloys. Although the designation of 'twin' vs. 'matrix' in the martensite is arbitrary, the narrower region was regarded as twin and the wider region as matrix. The width of transformation twins becomes finer with an increase in carbon content.

The most characteristic nature of thin plate martensite is that the M/A interface remains mobile. Figure 2.16 (Maki *et al*., 1989) shows

2.14 Transmission electron micrograph of thin plate martensite in Fe-30%Ni-0.39%C alloy (M_s = 133 K) (Maki and Tamura, 1986).

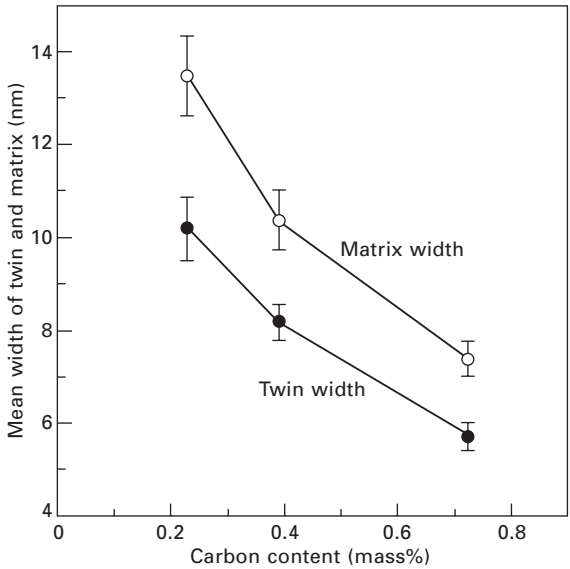

2.15 Change in twin width and matrix width in thin plate martensite with carbon content in Fe-Ni-C alloys (Maki and Wayman, 1976).

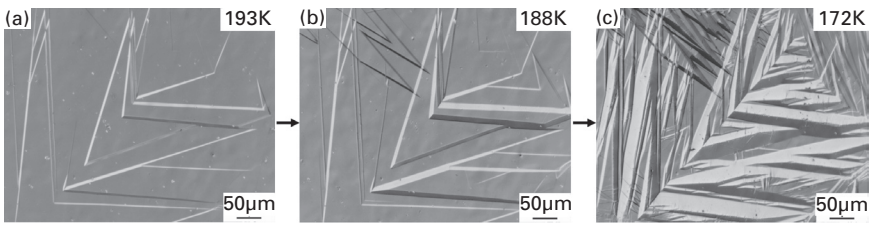

2.16 Optical micrographs showing transformation sequence of thin plate martensite during cooling in Fe-31%Ni-10%Co-3%Ti, ausaged at 873 K for 3.6 ks (M_s = 193 K) (Maki *et al.*, 1989).

the transformation sequence of thin plate martensite during cooling. It is evident that the thin plate martensite gradually thickens during cooling. This martensite also shrinks during heating by the backward movement of the A/M interface. This behaviour is not observed in other types of α' martensite. For example, in the case of lenticular martensite, each martensite plate attains the final size immediately when it forms, and no growth of the plate occurs by further cooling. Furthermore, the $\alpha' \rightarrow \gamma$ reverse transformation in lenticular martensite is always accomplished by the nucleation of austenite phase within a martensite plate rather than by the backward movement of interfaces (Kessler and Pitsch, 1965). The existence of fully extended transformation twins in martensite, and hence the smooth and planar interface, might thus be important for the reversible movement of the interface (Kajiwara and

Kikuchi, 1983). Because of this characteristic of interface movement during forward and reverse transformation, thin plate martensite has a possibility of exhibiting shape memory effect, such as in Fe-Pt (Wayman, 1971), Fe-Ni-Co-Ti (Maki *et al*., 1984), and Fe-Ni-Si (Himuro *et al*., 2002) alloys.

Judging from the characteristic of thin plate α′ martensite, i.e., completely twinned and perfect elastic accommodation in the parent austenite, the following four factors might be favourable for the formation of thin plate martensite in ferrous alloys

1. high austenite strength;
2. small transformation volume change and small magnitude of transformation shape change;
3. low M_s temperature (a low formation range); and
4. high tetragonality of martensite.

A high tetragonality of martensite corresponds to a small twinning shear, a low magnitude of shape strain, and low twin boundary energy (Kajiwara and Owen, 1977; Umemoto and Wayman, 1978). Thin plate α′ martensite has been observed in some ferrous alloys, such as Fe-high Ni-C (Maki *et al*., 1972), Fe-Ni-Al (Hornbogen and Mayer, 1967), Fe-7%Al-2.0%C (Watanabe and Wayman, 1971), Fe-25at%Pt (Umemoto and Wayman, 1978), Fe-Ni-Co-Ti (Maki *et al*., 1989), and Fe-Ni-Si (Himuro *et al*., 2002). These alloys have, more or less, some of the factors described above favourable for the formation of thin plate martensite. For example, all of the thin plate martensites in the above alloys have a fairly high tetragonality, and austenite strength that is also fairly high.

Since the interface of thin plate martensite is mobile, such martensite possesses the necessary condition for thermoelastic martensite. However, thin plate α′ martensite is not always thermoelastic, e.g., the thermal hysteresis (the temperature difference between M_s and A_s) of thin plate martensite in the Fe-Ni-C alloy shown in Fig. 2.14 is large, at about 600 K. Therefore, in order for thin plate α′ martensite to become thermoelastic, the introduction of suitable factors for reducing its thermal hysteresis is necessary. Dunne and Wayman (1973) found that the thermal hysteresis of thin plate martensite in Fe-25at%Pt alloy is gradually decreased with increase in the degree of order of the parent austenite and, hence, martensite can become thermoelastic with a small thermal hysteresis through a proper ordering treatment. Maki *et al*. (1984) also found that the Fe-Ni-Co-Ti alloys exhibit a thermoelastic martensite with a small thermal hysteresis when the austenite is properly aged to give the precipitation of γ′–Ni_3Ti. Judging from various previous observations, it can be considered that the important condition for reducing the thermal hysteresis of thin plate martensite is to reduce the thickness of the transformation twins in the martensite. High austenite strength and a high tetragonality of BCT martensite seem to be favourable for reducing twin

thickness in martensites. A high tetragonality leads to a substantial reduction in the energy of a twin boundary (Kajiwara and Owen, 1977). In fact, Fe-25at%Pt alloy (Dunne and Wayman, 1973) and Fe-33%Ni-10%Co-4%Ti alloy (Maki *et al*., 1984), which exhibit thermoelastic martensites, satisfy the conditions described above.

As mentioned above, morphologies of thin plate martensite and lenticular martensite are completely different from each other. However, when only the midrib in lenticular martensite is given attention, the substructure and habit plane of the midrib are quite similar to those of thin plate martensite. The similarity of morphology of midrib in lenticular martensite and thin plate martensite is shown in Fig. 2.17 (Shibata *et al*., 2008). As mentioned

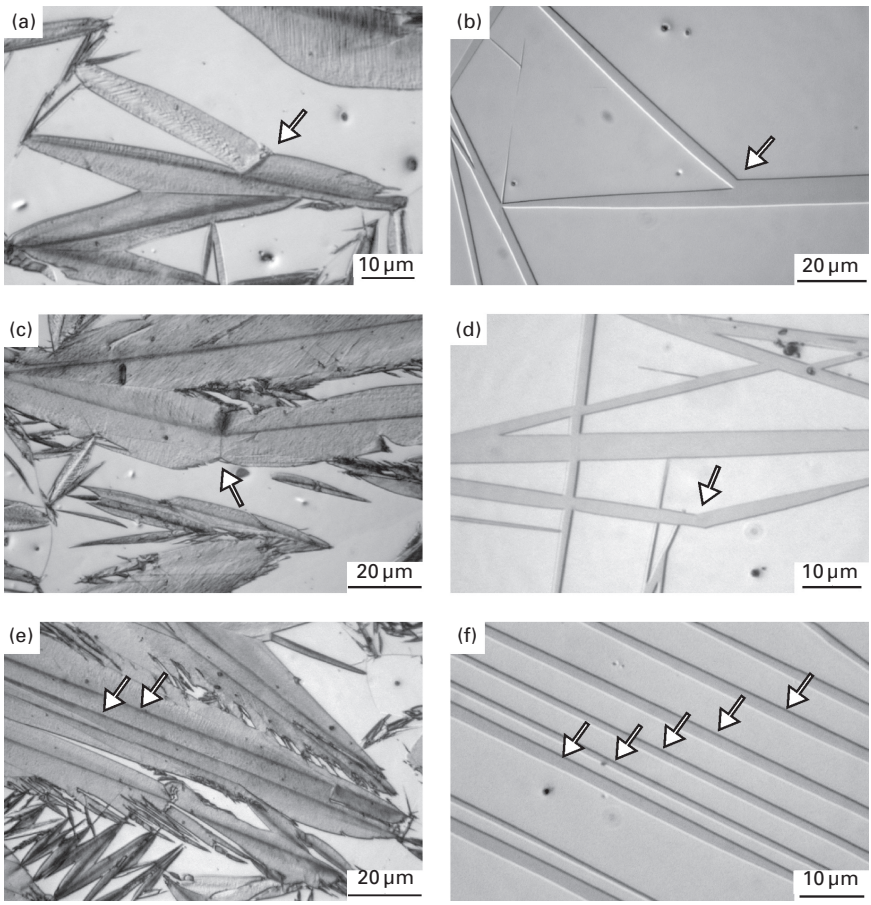

2.17 Optical micrographs showing various morphologies of lenticular martensite (Fe-29%Ni-0.2%C (M_s = 198 K)) (a, c and e), and thin plate martensite (Fe-31%Ni-10%Co-3%Ti (M_s = 83 K)) (b, d and e) (Shibata *et al*., 2008).

previously, lenticular martensite plates form in a group and exhibit a zigzag array (Fig. 2.1(d)). These arrays are quite similar to those of thin plate martensite (Fig. 2.1(e)). However, all lenticular martensite plates do not exhibit such a typical morphology, and some irregular morphologies often appear, as shown in Fig. 2.17(a), (c) and (e). The midrib in the lenticular martensite in Fig. 2.17(a) is branched, and that in Fig. 2.17(c) is kinked, as indicated by arrows. Unique morphologies such as these are often observed in thin plate martensite (Fig. 2.17(b) and (d)), as has been reported by Maki *et al*. (1973). Furthermore, single midrib does not always exist, and lenticular martensite plates with more than one midrib sometimes appear, as shown in Fig. 2.17(d). This configuration of midrib is quite similar to the morphology of thin plate martensite in Fig. 2.17(f), in which some martensite plates with the identical variant form closely with one another. Judging from the similarity of midrib and thin plate martensite, from the point of view of morphology, substructure and crystallographic features, it can be concluded that the midrib is thin plate martensite itself, and that the difference between lenticular martensite and thin plate martensite is only in their growth behaviour.

In order to confirm this consideration, the growth behaviour of thin plate martensite under applied stress at various temperatures was examined using an Fe-31%Ni-10%Co-3%Ti alloy (M_s = 83 K). Figure 2.18 (Shibata *et al*., 2008) summarizes the stress-induced growth behaviour of thin plate martensite by tensile deformation at various temperatures. The thermally transformed thin plate martensite grows whilst maintaining a thin plate shape when deformed below 110 K, but then grows into a lenticular shape above 160 K. In the temperature range between 110 and 160 K, both martensites with a thin plate shape or lenticular shape are observed. These results clearly indicate that the midrib in lenticular martensite is the thin plate martensite itself. Consequently, there is no difference between lenticular martensite at the earliest stage of martensite transformation (that is, the midrib) and thin plate martensite. When the formation temperature is quite low, martensite can grow whilst keeping a thin plate shape. On the other hand, when the formation temperature is relatively high, the change in deformation mode, from twinning to slip, results in the growth of martensite into a lenticular shape. This change in the lattice invariant deformation mode is due to the increase in the local temperature by latent heat during transformation. Although the local temperature is also raised in the case of thin plate martensite, the lattice invariant deformation mode remains twinning because of the relatively low formation temperature.

2.5 Conclusions

In this chapter, crystallographic features and substructure for various α' martensite with different morphologies, chiefly, lath, lenticular and thin plate,

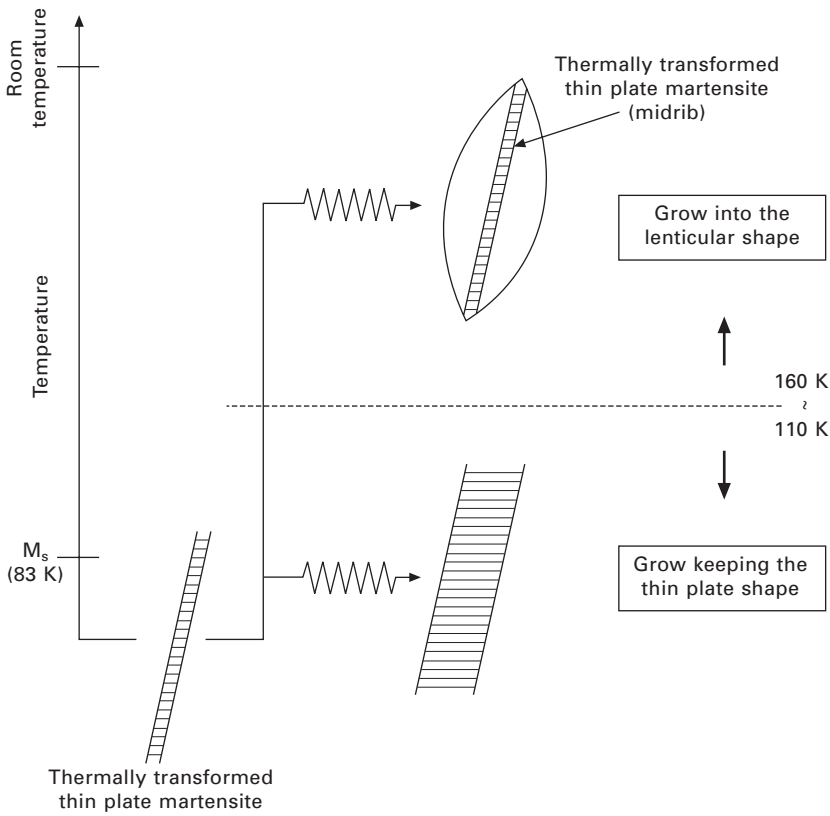

2.18 Schematic illustration showing stress-induced growth behaviour of thin plate martensites by tensile deformation at various temperatures in Fe-31%Ni-10%Co-3%Ti (M_s = 83 K). Specimen was cooled to liquid nitrogen (77 K) to form thin plate martensite and then deformed in tension at various temperatures between 77 K and 200 K (Shibata *et al.,* 2008).

were reviewed. In particular, the crystallographic features of packet and block in lath martensite, the origin of dislocation structure in lath and lenticular martensite, the substructure change during growth of martensite plate in lenticular martensite and the origin of midrib in lenticular martensite were described based on the author's recent studies. Studies on ferrous martensite were carried out extensively in the 1960s and 1970s. Irrespective of many previous studies, it remains the case that little quantitative investigation of substructure, e.g., dislocation and twin densities, the size of martensite lath, etc., has been reported. Further detailed and systematic studies of the substructure of martensite are necessary to understand the transformation mechanism and also the mechanical properties of the ferrous martensite.

2.6 References

Bowles J S and Mackenzie J K (1954), 'The crystallography of martensite transformations I', *Acta Metall.*, 2, 129–137.

Carr M J, Strife J R and Ansell G S (1978), 'An investigation of the effect of austenite strength and austenite stacking fault energy on the morphology of martensite in Fe-Ni-Cr-0.3C alloys', *Metall. Trans.*, *A*, 9A, 857–864.

Chaudhuri D K, Ravindran P A and Wert J J (1972), 'Comparative X-ray diffraction and electron microscopic study of the transformation-induced substructures in the iron-nickel martensites and their influence on the martensite properties', *J. Appl. Phys.*, 43, 778–788.

Davies R G and Magee C L (1971), 'Influence of austenite and martensite strength on martensite morphology', *Metall. Trans.*, 2, 1939–1947.

Dunne D P and Wayman C M (1973), 'The effect of austenite ordering on the martensite transformation in Fe-Pt alloys near the composition Fe_3Pt: morphology and transformation characteristic', *Metall. Trans.*, 4, 137–145.

Furuhara T, Kikumoto K, Saito H, Sekine T, Ogawa T, Morito S and Maki T (2008), 'Phase transformation from fine-grained austenite', *ISIJ Int.*, 48, 1038–1045.

Gourgues A F, Flower H M and Lindley T C (2000), 'Electron back scattering diffraction study of acicular ferrite, bainite, and martensite steel microstructures', *Mater. Sci. Tech.*, 16, 26–40.

Greninger A B and Troiano A R (1949), 'Mechanism of martensite formation', *Trans. AIME*, 185, 590–598.

Himuro Y, Kainuma R and Ishida K (2002), 'Martensitic transformation and shape memory effect in ausaged Fe-Ni-Si alloys', *ISIJ Int.*, 42, 184–190.

Hornbogen E and Mayer W A (1967), 'Gefüge und mechanische Eigenschaften von Legierungen auf Eisen-Nickel-Basis mit 12 at%Al nach verschiedener Wärmebehandlung', *Z. Metallk.*, 58, 372–380.

Inoue T, Matsuda S, Okamura Y and Aoki K (1970), 'The fracture of a low carbon tempered martensite', *Trans. JIM*, 11, 36–43.

Kajiwara S and Kikuchi T (1983), 'Reversible movement of the austenite-martensite interface and dislocation structures in reverse-transformed austenite in Fe-Ni-C alloys', *Phil. Mag. A*, 48, 509–526.

Kajiwara S and Owen W S (1977), 'The martensite-austenite interface and the thickness of twins in martensite in Fe_3Pt', *Scripta Metall.*, 11, 137–142.

Kakeshita T, Shimizu K, Maki T and Tamura I (1980), 'Growth behavior of lenticular and thin plate martensites in ferrous alloys and steels', *Scripta Metall.*, 14, 1067–1070.

Kehoe M and Kelly P M (1970), 'The role of carbon in the strength of ferrous martensite', *Scripta Metall.*, 4, 473–476.

Kessler H and Pitsch W (1965), 'Der Orientierungszusammenhang bei der Ruckumwandlung des Martensits in Austenit in Eisen-Nickel Legierungen', *Acta Metall.*, 13, 871–874.

Krauss G and Marder A R (1971), 'The morphology of martensite in iron alloys', *Metall. Trans.*, 2, 2343–2357.

Krauss G and Pitsch W (1965), 'Fine structure and habit planes of martensite in Fe-33wt% Ni single crystal', *Trans. AIME*, 233, 919–926.

Maki T (1990), 'Microstructure and mechanical behavior of ferrous martensite', *Mater. Sci. Forum*, 56–58, 157–168.

Maki T and Tamura I (1984), 'On the thin plate martensite in ferrous alloys and its various properties', *Bull. Japan Inst. Metals*, 23, 229–237.

Maki T and Tamura I (1986), 'Shape memory effect in ferrous alloys', *Proc. Int. Conf. on Martensitic Transformations (ICOMAT)*, JIM, pp. 963–970.

Maki T and Wayman C M (1976), 'Transformation twin width variation in Fe-Ni and Fe-Ni-C martensite', *Proc. 1st JIM Int. Symp. on New Aspects of Martensitic Transformation*, Kobe, JIM, pp. 69–74.

Maki T, Shimooka S, Umemoto M and Tamura I (1972), 'The morphology of strain-induced and thermally transformed martensite in Fe-Ni-C alloys', *Trans. JIM*, 13, 400–407.

Maki T, Shimooka S, Arimoto T and Tamura I (1973), 'The morphology of thin plate-like martensite in Fe-Ni-C alloys', *Trans. JIM*, 14, 62–67.

Maki T, Tsuzaki T and Tamura I (1980), 'The morphology of microstructure composed of lath martensite in steels', *Trans. ISIJ*, 20, 207–214.

Maki T, Kobayashi K, Minato M and Tamura I (1984), 'Thermoelastic martensite in an ausaged Fe-Ni-Ti-Co alloy', *Scripta Metall.*, 18, 1105–1109.

Maki T, Furutani S and Tamura I (1989), 'Shape memory effect related to thin plate martensite with large thermal hysteresis in ausaged Fe-Ni-Co-Ti alloy', *ISIJ Int.*, 29, 438–445.

Marder A R and Krauss G (1967), 'The morphology of martensite in iron-carbon alloys', *Trans ASM*, 60, 651–660.

Marder J M and Marder A R (1969), 'The morphology of iron-nickel massive martensite', *Trans. ASM*, 62, 1–10.

Matsuda S, Inoue T, Mimura H and Okamura Y (1972), 'Toughness and effective grain size in heat-treated low-alloy high strength steels', *Trans. ISIJ*, 12, 325–333.

Miyamoto G, Shibata A, Maki T and Furuhara T (2009), 'Precise measurement of strain accommodation in austenite matrix surrounding martensite in ferrous alloys by electron backscatter diffraction analysis', *Acta Mater.*, 57, 1120–1131.

Morito S, Tanaka H, Konishi R, Furuhara T and Maki T (2003a), 'The morphology and crystallography of lath martensite in Fe-C alloys', *Acta Mater.*, 51, 1789–1799.

Morito S, Nishikawa J and Maki T (2003b), 'Dislocation density within lath martensite in Fe-C and Fe-Ni alloys', *ISIJ Int.*, 43, 1475–1477.

Morito S, Saito H, Ogawa T, Furuhara T and Maki T (2005), 'Effect of austenite grain size on the morphology and crystallography of lath martensite in low carbon steels', *ISIJ Int.*, 45, 91–94.

Morito S, Huang X, Furuhara T, Maki T and Hansen N (2006), 'The morphology and crystallography of lath martensite in alloy steels', *Acta Mater.*, 54, 5323–5331.

Neuhauser H J and Pitsch W (1971), 'A new observation on the mechanism of martensitic transformations', *Acta Metall.*, 19, 337–344.

Norström L A (1976), 'On the yield strength of quenched low-carbon lath martensite', *Scand. J. Metall.*, 5, 159–165.

Ohmori Y, Ohtani H and Kunitake T (1974), 'Tempering of the bainite and the bainite/martensite duplex structure in a low-carbon low-alloy steel', *Met. Sci.*, 8, 357–366.

Oshima R, Sugimoto S, Sugiyama M, Hamada T and Fujita F E (1985), 'Shape memory effect in an ordered Fe_3Pt alloy associated with the FCC-FCT thermoelastic martensite transformation', *Trans. JIM*, 26, 523–524.

Patterson R L and Wayman C M (1966), 'The crystallography and growth of partially-twinned martensite plates in Fe-Ni alloys', *Acta Metall.*, 14, 347–369.

Reed R P (1967), 'The plate-like martensite transformation in Fe-Ni alloys', *Acta Metall.*, 15, 1287–1296.

Schumann H (1967), 'Die Martensitische Umwandlung in kohlenstoffarmen Manganstahlen', *Arch. Eisenfutt.*, 38, 647–656.

Shibata A, Murakami T, Morito S, Furuhara T and Maki T (2008), 'The origin of midrib in lenticular martensite', *Mater. Trans.*, 49, 1242–1248.

Shibata A, Morito S, Furuhara T and Maki T (2009), 'Substructures of lenticular martensites with different martensite start temperatures in ferrous alloys', *Acta Mater.*, 57, 483–492.

Shimizu K, Oka M and Wayman C M (1970), 'Transmission electron microscopy studies of $\{225\}_f$ martensite in an Fe-8%Cr-1%C alloy', *Acta Metall.*, 19, 1–6.

Sohmura T, Oshima R and Fujita F E (1980), 'Thermoelastic FCC-FCT martensitic transformation in Fe-Pd alloy', *Scripta Metall.*, 14, 855–856.

Swarr T E and Krauss G (1976), 'The effect of structure on the deformation of as-quenched and tempered martensite in an Fe-0.2%C alloy', *Metall. Trans. A*, 7A, 41–48.

Tsuzaki K and Maki T (1981), 'The effect of cooling rate on the morphology of lath martensite in Fe-Ni alloys', *J. Japan Inst. Metals.*, 45, 126–134.

Umemoto M and Wayman C M (1978), 'The effect of austenite ordering on the transformation temperature, transformation hysteresis, and thermoelastic behavior in Fe-Pt alloys', *Metall. Trans. A*, 9A, 891–897.

Umemoto M, Hyodo T, Maeda T and Tamura I (1984), 'Electron microscopy studies of butterfly martensite', *Acta Metall.*, 32, 1191–1203.

Watanabe M and Wayman C M (1971), 'Crystallography of the martensite transformation in Fe-Al-C alloys', *Metall. Trans.*, 2, 2229–2236.

Wayman C M (1971), 'On memory effect related to martensitic transformations and observations in b-brass and Fe_3Pt', *Scripta Metall.*, 5, 489–492.

Wechsler M S, Lieberman D S and Read T A (1953), 'On the theory of the formation of martensite', *Trans AIME*, 197, 1503–1515.

Zaefferer S (2003), 'Computer-aided crystallographic analysis in the TEM', *Adv. in Imaging and Electron Physics*, 125, 355–415.